Chapter 4

AlAs/$In_{0.53}Ga_{0.47}As$ Quantum Well Injection Transit (QWITT) Diodes

Although the DBRTDs discussed so far have found application in high speed circuits, their ability to generate useful amounts of power in microwave oscillators is rather limited. The oscillator output power is proportional to the $\Delta V \Delta J$ product. In the previous chapter it was shown that by adopting the $AlAs/In_{0.53}Ga_{0.47}As$ material system, higher output powers could be achieved due to the larger ΔJ available. In this chapter we discuss the possibility of increasing ΔV while maintaining this improvement in ΔJ. Referring back to the conduction band energy diagram of Fig. 3.1(c), one can see that a depletion region is formed downstream of the quantum well. Since a substantial fraction of the applied voltage is dropped across this region, it is reasonable to expect that modifying the spacer layers in this downstream region will affect the J - V characteristics, and in particular, the voltage axis. A variation of the baseline DBRTD that exploits electron transport through the downstream spacer layers is the Quantum Well Injection Transit (QWITT) diode, proposed by Kesan *et al.* [1]. In this chapter we discuss the design and optimization of DBRTDs for microwave oscillator applications.

4.1 Introduction

A layer schematic of the QWITT diode is given in Fig. 4.1. The device is divided into two regions. The region on the emitter (cathode) side of the device up to and including the double barrier quantum well structure is called the injector. The moderately doped thick spacer layer, of thickness W, on the collector (anode) side forms the drift region. The electric field in the drift region is assumed to be high enough to cause the injected electrons to traverse the drift region at a constant saturation velocity, v_{sat}.

For purposes of analysis we decouple the semi-classical transport occurring in the drift region from the quantum interference effects occurring in the quantum well [[2]]. The influence of the drift region can then be understood by characterizing the injector with an injection characteristic. This characteristic, shown in Fig. 4.2, describes the current through the device as a function of the electric field at the boundary separating the injector and the drift region.

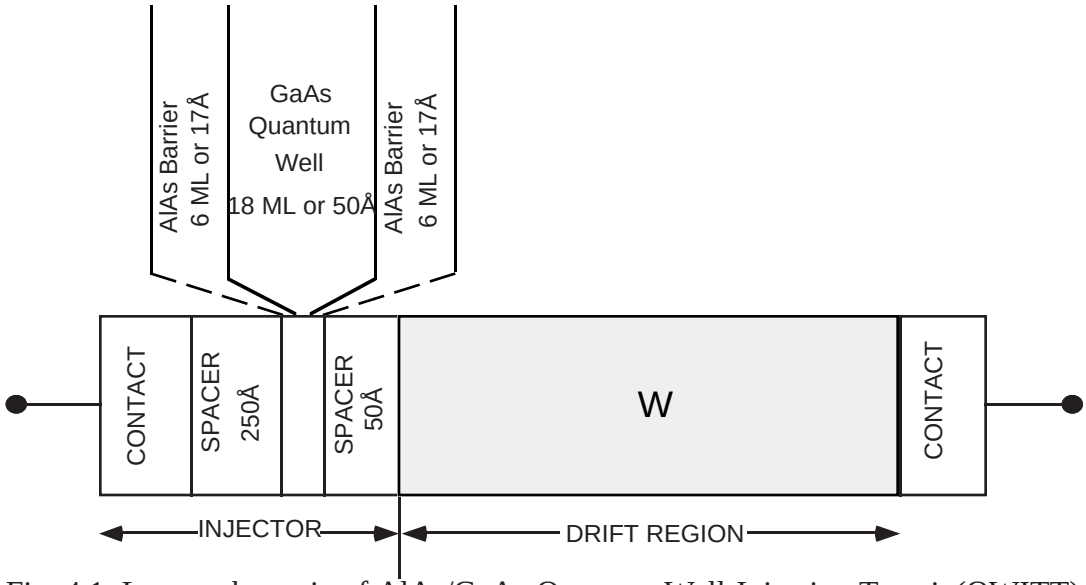

Fig. 4.1 Layer schematic of AlAs/GaAs Quantum Well Injection Transit (QWITT) diode. The device is divided into two sections, the quantum well injector and the drift region, of length W, over which a significant fraction of the applied voltage is dropped. The cathode is the left contact and current is assumed to be carried by electrons.

Since the device is biased in the NDR region, the quantum well injector can be characterized by a normalized injection conductance, σ, which is given by

$$\sigma = \frac{\partial J}{\partial E} = \frac{\Delta J}{\Delta E} \tag{4.1}$$

where the NDR characteristic was assumed to be linear between the peak and valley.

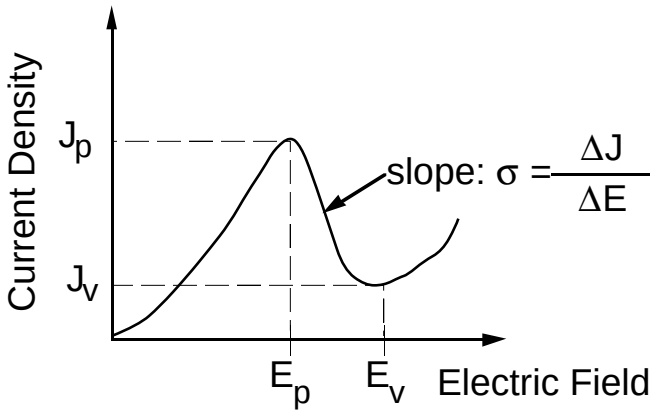

Fig. 4.2 Current density versus electric field (J - E) characteristics of the DBRTD quantum well. Under the assumption that the drift region carrier transport is at a constant saturation velocity, independent of the injection characteristic, the J - E curve can be extracted from the DBRTD J - V characteristic by accounting for the voltage drop due to the depleted spacer layers and ohmic contact resistance.

We can now see how increasing the drift region or spacer layer width on the anode side should affect ΔV. Shown in Fig. 4.3 are the electric field profiles in the drift region corresponding to the peak and valley points of the J - E injector characteristic.

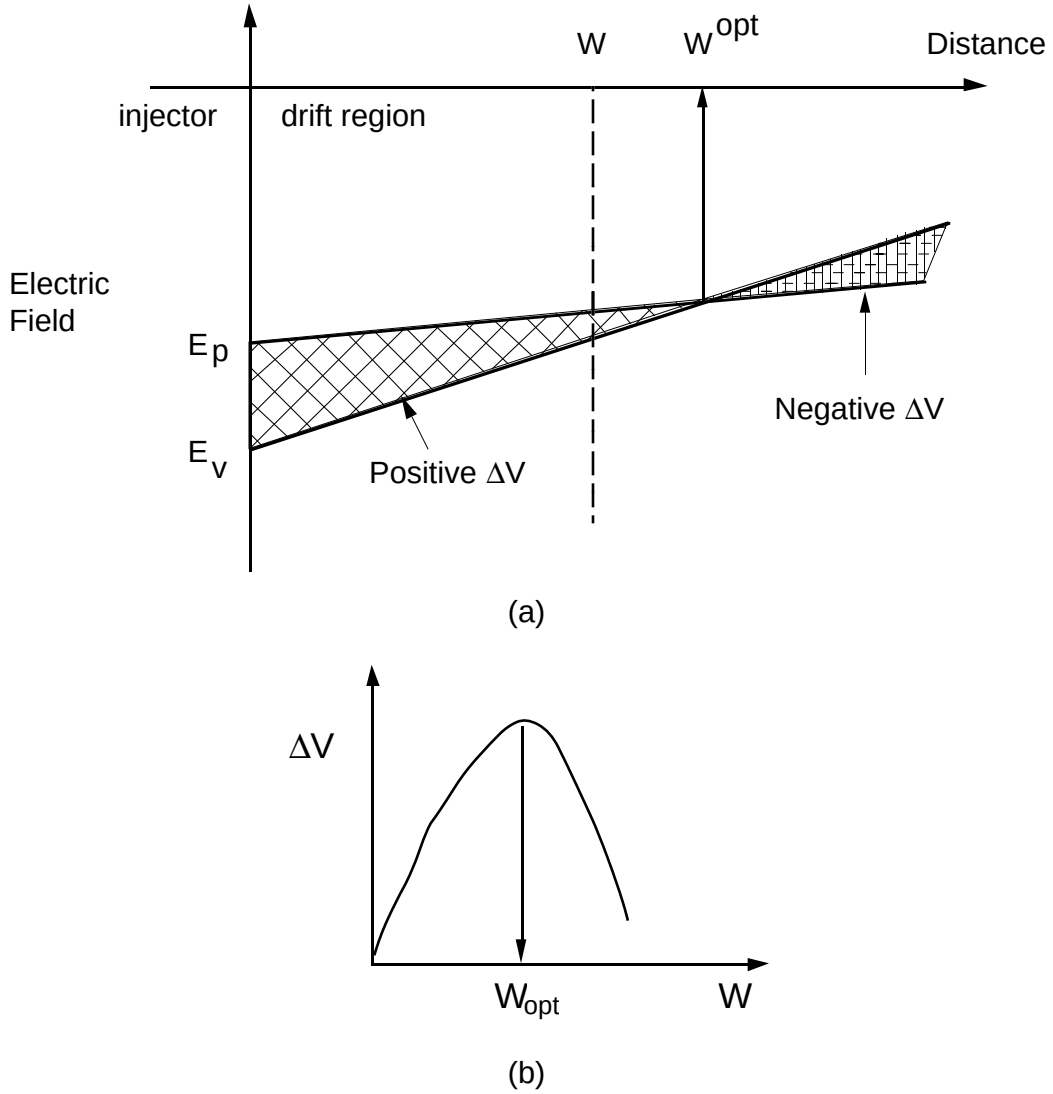

Fig. 4.3 (a) A qualitative illustration of the electric field profiles in the drift region corresponding to the peak and valley points of the injector characteristic of Fig. 4.2. W is the drift region length. The positive slope, from Poisson's equation, represents the case where the injected electron density necessary to support the current is less than the background doping. (b) The voltage ΔV is just the shaded area between the peak and valley electric field curves and is maximized at an optimum drift region length, W_{opt}.

The slope of the electric field is positive, which from Poisson's equation, represents the case where the injected electron density necessary to support the current is less than the background doping density, as shown below

$$\frac{\partial E}{\partial x} = \frac{q}{\varepsilon}\left(N_d^+ - \frac{J}{q v_{sat}} \right) \tag{4.2}$$

where J is the current density through the device and N_d is the background dopant concentration. The slope of the field at the valley is greater than that at the peak because the current density, and thus the electron concentration, is lower in the valley. The voltage ΔV, the difference in the peak and valley voltages, is just the shaded area between the peak and valley electric field curves. Therefore, by increasing W from the baseline value of 250Å, one can increase the ΔV.

Figure 4.4 shows measured J - V characteristics for a baseline AlAs/$In_{0.53}Ga_{0.47}As$ DBRTD (W = 300Å) and an AlAs/$In_{0.53}Ga_{0.47}As$ QWITT with a drift region length of 1000Å. The emitter spacer layers and quantum well in both devices are nominally identical. The quantum well consists of 17Å AlAs barriers and a 50Å $In_{0.53}Ga_{0.47}As$ well. The emitter spacer layers, beginning with the closest to the quantum well, are 50Å nominally undoped $In_{0.53}Ga_{0.47}As$ (n-type 5 x 10^{15} cm^{-3}), 100Å (4 x 10^{16} cm^{-3}) $In_{0.53}Ga_{0.47}As$, and finally 100Å (2 x 10^{17} cm^{-3}) $In_{0.53}Ga_{0.47}As$. The ΔV for the baseline DBRTD is only 0.5 V. But by increasing the drift length to 1000Å the ΔV is doubled to approximately 1.0 V. Since ΔV is increased while ΔJ remains essentially the same, the specific negative resistance increases over that of the baseline DBRTD. This increased negative resistance relaxes circuit impedance matching constraints and allows the use of larger area devices. Therefore much higher RF output powers can be obtained with QWITT diodes.

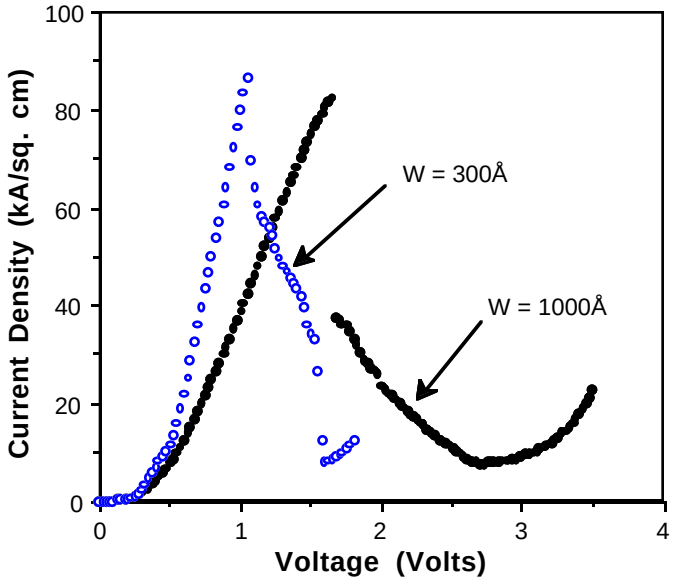

Fig. 4.4 Measured J - V characteristics of baseline AlAs/$In_{0.53}Ga_{0.47}As$ DBRTD with W=300Å and W=1000Å, AlAs/$In_{0.53}Ga_{0.47}As$ QWITT. The quantum well in both devices consists of 17Å AlAs barriers and 50Å $In_{0.53}Ga_{0.47}As$ well. The ΔV for the baseline DBRTD and QWITT are 0.5 V and 1.0 V, respectively. The injection conductance, σ, for these devices is -0.5 $(ohm\text{-}cm)^{-1}$. Since the ΔV has doubled while ΔJ remains essentially the same, the specific negative resistance is effectively doubled over that of the DBRTD.

However, increasing W arbitrarily is not recommended. As shown in Fig. 4.3, there exists an optimum drift region length, W_{opt}, at which the maximum ΔV is obtained (where the electric field profiles intersect). In the next section, an expression for W_{opt} will be derived in terms of the quantum well injector characteristic, σ, and the saturation velocity in the drift region, v_{sat}.

The decoupling of the injector from the drift region is a good assumption since the injector characteristic should not depend on the drift region design. It is, however, influenced by the thin spacer layers on the emitter side of the quantum well. A dramatic example of this is the zero-bias, multi-state DBRTD recently reported by Gullapalli *et al.* [3]. The advantage of lumping the complex physics of the quantum well into an injection conductance is that the drift region and the quantum well can be independently optimized and the effects of each region on the other can be conveniently studied.

4.2 QWITT Linear J - E Model

For oscillator circuit design an accurate expression for the device impedance must be obtained. In the QWITT structure, it is assumed that the quantum well region length is much smaller than the drift region length. As will be shown later, typical drift regions lengths vary from 1000Å to 1 μm, which is much larger than the typical quantum well region length of approximately 100Å. Therefore, the device impedance is dominated by the drift region.

The drift region impedance, Z_d, can be calculated by integrating the drift region electron field and dividing by the current to obtain the specific impedance and is given by [4],[5]

$$Z_d = \frac{W}{j\omega\varepsilon}\left[1 - \frac{\sigma}{\sigma + j\omega\varepsilon}\,\frac{1-\exp(-j\theta_d)}{j\theta_d}\right] \tag{4.3}$$

where ω is the angular frequency and θ_d is the drift angle, given by $\theta_d = \omega W/v_{sat}$. The above equation was derived assuming that the carriers were traversing the drift region at a constant saturation velocity. The specific resistance, given by the real part of Z_d, is:

$$R_d = 2\left(\frac{v_{sat}\varepsilon}{2\sigma^2}\right)\left[1-\cos\left(\frac{\omega W}{v_{sat}}\right)+\frac{\omega}{\sigma/\varepsilon}\sin\left(\frac{\omega W}{v_{sat}}\right)\right]\left(\frac{\omega}{\sigma/\varepsilon}\right)^{-2}\left[1+\left(\frac{\omega}{\sigma/\varepsilon}\right)^2\right]^{-1} \qquad (4.4)$$

The behavior of Eq. 4.4 depends significantly on the sign of σ. For positive σ, the negative resistance is narrow band as in conventional transit-time devices [6]. However, for negative σ (when the device is biased in the NDR region), R_d exhibits very interesting characteristics as a function of frequency. The frequency behavior can be divided into two frequency ranges, $\omega << |\sigma|/\varepsilon$ and $\omega >> |\sigma|/\varepsilon$, where $|\sigma|/\varepsilon$ is a characteristic frequency of the device.

For $\omega << |\sigma|/\varepsilon$, R_d is independent of frequency

$$R_d = \frac{W}{\sigma} + \frac{W^2}{2\varepsilon v_{sat}} \qquad (4.5)$$

The first term in Eq 4.5 is negative since σ is negative. The second term is always positive and represents the space-charge resistance familiar in conventional transit-time device theory. The total R_d will be negative if $W < 2\varepsilon v_{sat}/|\sigma|$. It will be shown on the next page that Eq. 4.5 can also be found in a different manner that highlights the significant space charge effects arising from carrier transit in a space-charge region.

For $\omega >> |\sigma|/\varepsilon$, R_d is frequency dependent and given by:

$$R_d = \frac{v_{sat}\sigma}{\varepsilon^2\omega^3}\sin\left(\frac{\omega W}{v_{sat}}\right) \qquad (4.6)$$

For frequencies below $|\sigma|/\varepsilon$, the QWITT diode exhibits a constant, broad band negative resistance and for frequencies much greater than $|\sigma|/\varepsilon$, the resistance falls rapidly as ω^{-3}. Therefore, it is desirable to operate the device in the "low

frequency" regime where the negative resistance is constant and avoid the ω^{-3} falloff at frequencies much greater than $|\sigma|/\varepsilon$.

The QWITT diode was originally conceived as a "conventional" transit-time device and the acronym stood for Quantum Well Injection Transit-Time. The operation of transit-time devices, in the conventional sense, usually requires that the phase delay due to carrier transit-time in the drift region be a significant fraction of the ac voltage cycle. For example, devices such as the impact-ionization avalanche transit-time (IMPATT) diode operate only in a narrow frequency band where the carrier transit-time is approximately half of the ac voltage cycle (i.e., the drift angle, $\omega W/v_{sat}$, is π). In the QWITT diode when $\sigma > 0$, the device exhibits narrow-band negative resistance similar to other transit-time devices only when the drift angle (for optimum σ) is $5\pi/3$ [4]. Thus, in this regard, it is similar to a conventional transit time device.

However, when σ is negative, as it can be in a QWITT diode, the situation is quite different. For $\omega << |\sigma|/\varepsilon$, the optimum depletion layer thickness is independent of frequency, which is a unique feature not seen in positive injection conductance devices such as IMPATTs. This is true even if the transit angle (i.e., delay) is much less than the ac period. The utilization of the drift region in QWITT diodes is very different from the use of carrier "delay" effects in devices such as IMPATTs. The negative resistance enhancement in the QWITT diode is simply due to the fact that the injection conductance is negative and the electric field is allowed to drop over a drift region. However the carrier density modulation in the transit region prevents unlimited increase in the negative resistance of the device and counteracts the beneficial effects of negative injection conductance. Hence there exists an optimum W (W_{opt}, see Fig. 4.3) for maximum negative resistance for a given σ. This in essence is the QWITT diode, and to highlight this fact and avoid confusion with the conventional notion of 'transit-time,' the word 'time' is dropped from the name. It should be pointed out that all transit time analysis for IMPATTs and QWITTs is valid as a function of frequency, regardless of the drift

angle magnitude compared to 2π. But, only if σ is negative can the negative resistance increase even when the drift angle is much less than 2π.

To illustrate the above discussion, a dc analysis that takes into account space-charge modulation effects can be used to find Eq. 4.5 and shed insight into the effect of the drift region on the J - V characteristics [7]. Consider the geometry of Fig. 4.1 where the device is divided into an injector, characterized with an injection conductance σ, and a fully depleted drift region of length W (through which carriers move at a constant velocity v_{sat}). The magnitude of the electric field as a function of position, $E_1(z)$ at a constant current density J_1 is:

$$E_1(z) = E_0 - \frac{q}{\varepsilon}\left(N_d^+ - \frac{J_1}{q v_{sat}}\right)z \tag{4.7}$$

where E_o is the electric field at the injecting plane z = 0, the boundary between the injector and the drift region. With a perturbation in the form of additional current ΔJ, the resultant electric field, $E_2(z)$ profile is given by

$$E_2(z) = \left(E_0 + \Delta E\right) - \frac{q}{\varepsilon}\left(N_d^+ - \frac{J_1 + \Delta J}{q v_{sat}}\right)z \tag{4.8}$$

The corresponding change in voltage across the drift region to first order in ΔJ is then

$$\Delta V = \int_0^W \left(E_2(z) - E_1(z)\right)dz = W\Delta E + \frac{W^2 \Delta J}{2\varepsilon v_{sat}} \tag{4.9}$$

where W is assumed to remain the same before and after the current perturbation. Dividing both side by ΔJ, one arrives at an expression for the differential resistance $\Delta V/\Delta J$ across the drift region:

$$R = \frac{\Delta V}{\Delta J} = \frac{W}{\sigma_{inj}(E_o)} + \frac{W^2}{2\varepsilon v_{sat}} \tag{4.10}$$

where

$$\sigma_{inj}(E_0) = \left.\frac{\partial J_i}{\partial E_i}\right|_{E_0} \tag{4.11}$$

Equation 4.10 is identical to Eq. 4.5, which was derived from the drift-diffusion transport equations. This resistance is the ratio of the change in voltage across the depletion layer to the change in current density. Since it is desirable to operate the QWITT diode in the "low frequency" limit where $\omega << |\sigma|/\varepsilon$, one can attempt to maximize the negative resistance given by Eq. 4.10. For a given σ and v_{sat}, the optimum drift region length, W_{opt}, for maximum negative resistance is given as

$$W_{opt} = \frac{\varepsilon v_{sat}}{\sigma} \tag{4.12}$$

As shown earlier in Fig. 4.3, W_{opt} is the drift region length at which ΔV is maximum. From Eq. 4.11, we see there are two ways to increase W_{opt}: decrease σ or increase v_{sat}. By decreasing σ, one reduces the characteristic frequency, $|\sigma|/\varepsilon$, and thus the frequency range over which the negative resistance is constant. Increasing v_{sat} is possible by adjusting the material composition of the drift region. However, lattice-matching requirements restrict the choice of drift region material composition. AlAs/GaAs and AlAs/$In_{0.53}Ga_{0.47}As$ QWITTs require the drift region to be GaAs or AlGaAs and $In_{0.53}Ga_{0.47}As$, respectively. Therefore, v_{sat} is fixed by the drift region composition, where the saturation velocity for GaAs and $In_{0.53}Ga_{0.47}As$ is 6 x 10^6 cm/sec and 5 x 10^6 cm/sec, respectively [8],[9].

4.3 AlAs/$In_{0.53}Ga_{0.47}As$ QWITTs

As discussed earlier, the QWITT diode offers a larger ΔV and hence larger negative resistance than a baseline DBRTD. This is achieved by replacing the thin spacer layers on one side of the quantum well with a longer, moderately doped drift region. Taking advantage of the higher ΔJ's available with the AlAs/$In_{0.53}Ga_{0.47}As$ material system, QWITT diodes were fabricated and characterized.

Shown in Fig. 4.5 is the layer schematic of high current density AlAs/$In_{0.53}Ga_{0.47}As$ QWITTs. The quantum well consists of 6 ML AlAs barriers and a 50Å $In_{0.53}Ga_{0.47}As$ well. Three devices were fabricated and tested: a baseline DBRTD and two QWITTs (W = 1000Å and W = 2000Å). The upstream spacer layer doping concentrations and dimensions are similar to the AlAs/$In_{0.53}Ga_{0.47}As$ DBRTDs discussed in chapter 3. Downstream, the spacer layers varied as follows. For the baseline DBRTD, W = 200Å and consisted of 100Å ($n = 5.1 \times 10^{16}$ cm^{-3}) and 100Å ($n = 1.9 \times 10^{17}$ cm^{-3}). For the first QWITT, W = 1000Å with a drift region doping concentration of 2.5×10^{17} cm^{-3}. For the second QWITT, the drift region length was increased to 2000Å while the doping remain unchanged.

500Å	3.6 x 10^{18} cm^{-3}	InGaAs
2500Å	2.1 x 10^{18} cm^{-3}	InGaAs
100Å	1.9 x 10^{17} cm^{-3}	InGaAs
100Å	5.1 x 10^{16} cm^{-3}	InGaAs
50Å	Undoped	InGaAs
6 ML	Undoped	AlAs
50Å	Undoped	InGaAs
6 ML	Undoped	AlAs
50Å	Undoped	InGaAs
W	N_{Drift}	InGaAs
3000Å	2.1 x 10^{18} cm^{-3}	InGaAs
	n+ InP substrate	

Fig. 4.5 Layer schematic of AlAs/$In_{0.53}Ga_{0.47}As$ DBRTD and QWITTs. Three devices were fabricated and tested, a baseline DBRTD and two QWITTs (W = 1000Å and W = 2000Å). For the baseline DBRTD, W = 200Å and consisted of 100Å (n = 5.1 x 10^{16} cm^{-3}) and 100Å (n = 1.9 x 10^{17} cm^{-3}). For the first QWITT, W = 1000Å with a N_{Drift} = 2.5 x 10^{17} cm^{-3}. For the second QWITT, the drift region length was increased to 2000Å with the same N_{Drift}.

Shown in Fig. 4.6 are the measured J - V characteristics of the three AlAs/$In_{0.53}Ga_{0.47}As$ devices. Under forward bias the W = 1000Å and the W = 2000Å characteristics are almost identical while the baseline DBRTD exhibits a J_p higher than that of the QWITT diodes. This is due to the fact that under forward

bias, the drift region (which is upstream from the quantum well) forms a barrier to electron flow due to the junction potential between the heavily doped contact layer and the undoped quantum well [10]. For the heavy contact doping concentrations present in these devices, the upstream electron supply function is affected by the distance between the heavily doped contact layer and the quantum well. Therefore, as W is increased the effective electron concentration available for tunneling is reduced and hence the peak current density is reduced. The magnitude of this bias asymmetry in J_p depends on the contact layer doping concentration. Reducing the concentration will reduce the asymmetry but this will also result in lower J_p since the electron supply is also reduced. However, since QWITT diodes will be reverse biased during oscillator operation, this asymmetry in J_p is not really of concern.

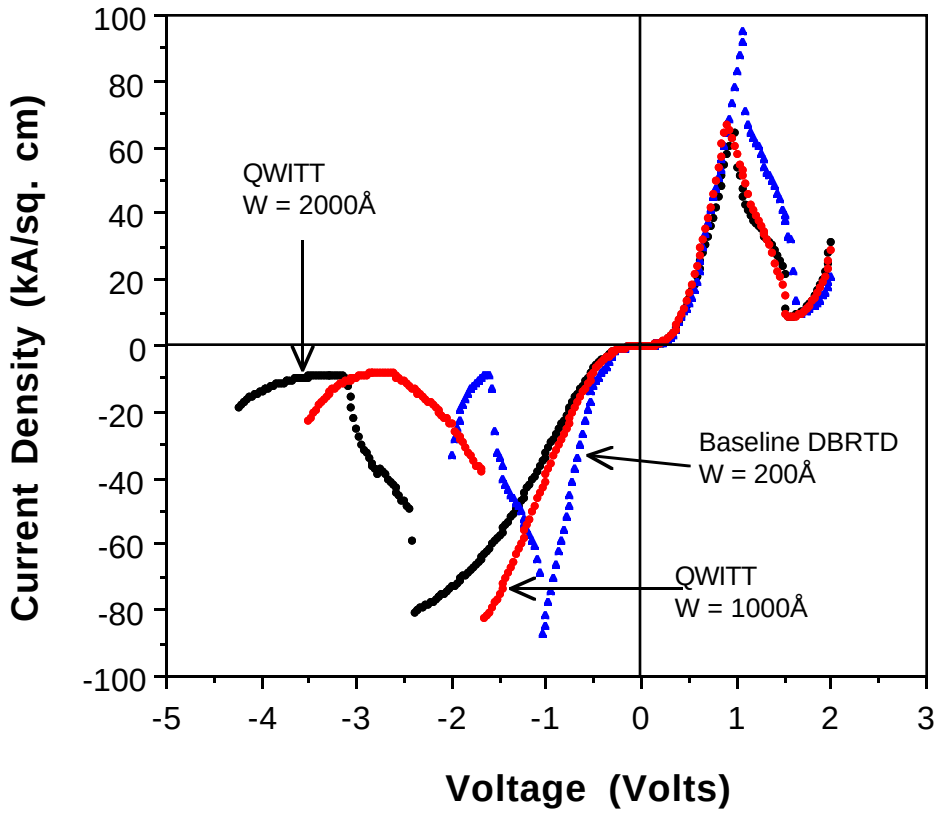

Fig. 4.6 Measured J - V characteristics of the three AlAs/$In_{0.53}Ga_{0.47}As$ devices: Baseline DBRTD (W = 200Å), QWITT (W = 1000Å), and QWITT (W = 2000A). The injection conductance, σ, is -0.5 $(ohm\text{-}cm)^{-1}$.

In reverse bias (QWITT mode), the characteristics are quite interesting. As expected J_p and ΔJ are similar for all three structures since the upstream spacer layers are nominally identical. Also, V_p increases as the drift region length increases as expected. However, ΔV does not increase with W indefinitely. Recall from Fig. 4.3 and Eq. 4.12 that there exists a W_{opt} at which maximum ΔV is obtained. If the ΔV of the devices shown in Fig. 4.6 is plotted as function of W, then Fig. 4.7 results. A few comments should be made regarding how the data is plotted. First, 50 Å has been added to all the depleted drift region lengths to

account for the 50Å undoped layer adjacent to the AlAs barrier. Second, analysis of the J - V data of the W = 2000Å QWITT data with a Poisson solver revealed that only 1300Å had been depleted. The remaining 700Å was undepleted because the drift region doping concentration of 2.5 x 10^{17} cm^{-3} was probably too high for the quantum well electric fields involved.

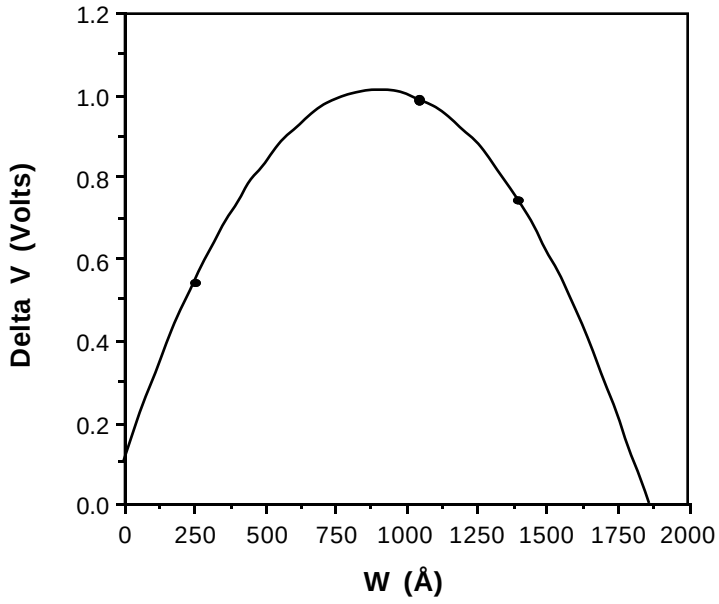

Fig. 4.7 ΔV vs W for AlAs/$In_{0.53}Ga_{0.47}As$ QWITTs. There exists a W_{opt} = 900Å at which maximum ΔV can be obtained. For W = 0Å, ΔV = 0.11V which is due to the voltage drop across the quantum well.

Fig. 4.7 shows the expected inverse parabolic shape (Eq. 4.9) and the drift region at which maximum ΔV is obtained, W_{opt}, is calculated to be approximately 900Å. The maximum ΔV possible is about 1 V and is achieved with the W = 1000Å QWITT diode. Assuming a v_{sat} of 5 x 10^6 cm/s and a relative dielectric constant of 13.5 for $In_{0.53}Ga_{0.47}As$, the σ computed from Eq. 4.11 is -0.66 $(ohm\text{-}cm)^{-1}$. This is good agreement with the σ extracted from the J - V characteristics.

The non-zero ΔV at W = 0Å of 0.11V is due to voltage drop across the quantum well. The injection conductance can also be calculated from this data point to be:

$$\sigma = \Delta J \frac{L_{QW}}{\Delta V_{W=0\,Å}} \tag{4.13}$$

where L_{QW} is the quantum well length. Plugging ΔJ = 75 kA/cm^2 and L_{QW} = 83Å into Eq. 4.13, σ = -0.57 (ohm-cm)$^{-1}$. As a further check of self-consistency, the v_{sat} calculated from Eq. 4.11 where W_{opt} is taken to be 900Å and σ is taken from Eq. 4.12, is computed to be 4.3 x 10^6 cm/s, close to the expected value of 5 x 10^6 cm/s. Taking the average of the three σ's calculated above to define the intrinsic quantum well conductance, we find that σ = -0.58 (ohm-cm)$^{-1}$.

4.4 AlAs/$In_{0.53}Ga_{0.47}As$ QWITTs: Effect of drift region doping

We have seen in the previous section that the optimum drift region length to obtain maximum ΔV depends on the quantum well injection conductance. Another parameter that can significantly affect the J - V characteristics is the drift region doping, N_{Drift}. It should not be too high as to not allow complete depletion of the drift layer, as was the case for the W = 2000Å QWITT discussed earlier. On the other hand, too low a doping can have deleterious and even catastrophic effects. To study the effect of varying the drift region doping on the J - V characteristics, three AlAs/$In_{0.53}Ga_{0.47}As$ QWITTs were fabricated with their layer schematic given in Fig. 4.8. Three diodes were fabricated with N_{Drift} = 3.4 x 10^{17} cm^{-3} (QWITT A), 2x10^{17} cm^{-3} (QWITT B), and 8.6 x 10^{16} cm^{-3} (QWITT C). The drift region length is 1000Å and the quantum well consists of a 47Å $In_{0.53}Ga_{0.47}As$ well and 6 ML AlAs barriers.

The measured J - V characteristics are shown in Fig. 4.9 with forward bias being the non-QWITT mode. As expected, the forward bias characteristics are similar since the upstream dopant profiles are nominally identical.

500Å	2.6 x 10^{18} cm^{-3}	InGaAs
3000Å	1.6 x 10^{18} cm^{-3}	InGaAs
100Å	2.0 x 10^{17} cm^{-3}	InGaAs
100Å	2.0 x 10^{16} cm^{-3}	InGaAs
50Å	Undoped	InGaAs
6 ML	Undoped	AlAs
47Å	Undoped	InGaAs
6 ML	Undoped	AlAs
50Å	Undoped	InGaAs
1000Å	N_{Drift}	InGaAs
3000Å	2.0 x 10^{18} cm^{-3}	InGaAs
	n+ InP substrate	

Fig. 4.8 Layer schematic of AlAs/$In_{0.53}Ga_{0.47}As$ QWITTs fabricated to study the effects of drift region doping, N_{Drift}, on the J - V characteristics. Three diodes were grown with N_{Drift} = 3.4 x 10^{17} cm^{-3} (QWITT A), 2x10^{17} cm^{-3} (QWITT B), and 8.6 x 10^{16} cm^{-3} (QWITT C).

Comparing QWITT A and QWITT B under reverse bias, we see that as N_{Drift} is reduced the peak voltage increases but the ΔV remains the same,

approximately 1 V. Such behavior is expected since, as long the drift region is fully depleted ΔV should remain unchanged but the peak voltage will increase due to the lower doping in the drift region. However, if the drift region doping is reduced too much, the electron concentration required to support the peak current density can become greater than the background doping concentration. Such a situation occurs with QWITT C, which breaks down at very near the peak voltage, roughly -2.8 V, and the current density at this point is -110 kA/cm^2. The equivalent electron concentration at this current density is 1.4 x 10^{17} cm^{-3} (assuming v_{sat} = 5 x 10^6 cm^{-3}). Since the electron concentration is greater than the background concentration of 8.6 x 10^{16} cm^{-3}, the magnitude of the electric field increases in the drift region rather than decreasing.

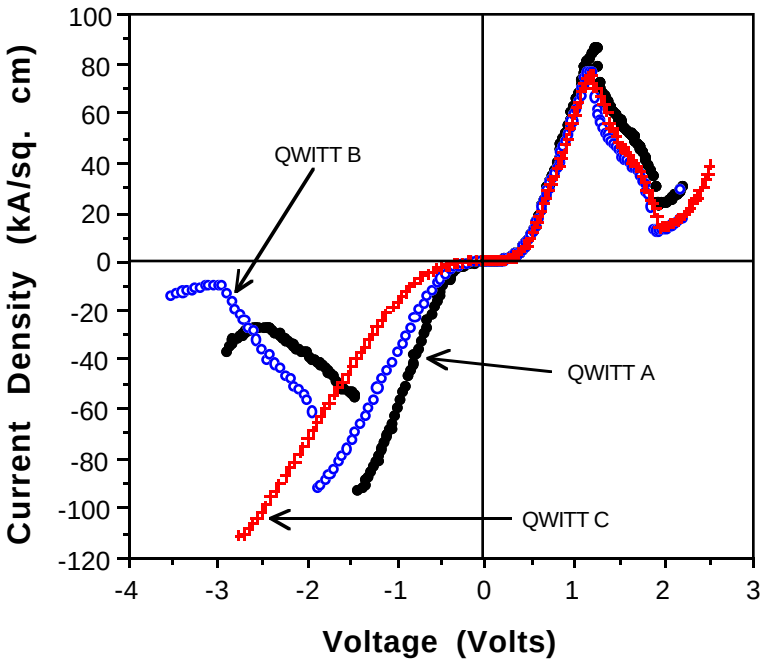

Fig. 4.9 Measured J - V characteristics of AlAs/$In_{0.53}Ga_{0.47}As$ QWITTs with different drift region doping concentrations: QWITT A (3.4 x 10^{17} cm^{-3}), QWITT B (2x10^{17} cm^{-3}), and QWITT C (8.6 x 10^{16} cm^{-3}).

The physical breakdown process is unclear at present. One plausible mechanism leading to breakdown involves impact ionization events in the drift region [[11]]. This is particularly true for $In_{0.53}Ga_{0.47}As$ which has a relatively narrow bandgap of 0.75 eV, whereas GaAs has a bandgap of 1.42 eV. Therefore, impact ionization is expected to be quite important and must be considered in high current density devices [[12]]. Electrons entering the drift region gain energy from the rising electric field and participate in impact ionization. This results in more electrons in the drift region which contribute to increasing the electric field and this positive feedback process eventually leads to breakdown. The holes that are created from the impact ionization events will drift towards the quantum well and may become trapped at the valence band hetero-junction between the AlAs barrier and the $In_{0.53}Ga_{0.47}As$ drift region. The presence of positively charged holes will then locally enhance the electric field at this hetero-junction and also result in a positive feedback process again leading to breakdown. Admittedly, the above arguments are speculative and rigorous self-consistent models incorporating accurate impact ionization models are required to understand the breakdown mechanism. From an device design point of view, the above concerns can be avoided by ensuring that the drift region doping is sufficiently higher than the peak electron concentration.

4.5 AlAs/$In_{0.53}Ga_{0.47}As$ QWITTs: low sigma devices

In addition to investigating high σ QWITTs, low σ devices were also studied. Two AlAs/$In_{0.53}Ga_{0.47}As$ QWITTs were fabricated and their layer schematic is given in Fig. 4.10. These devices are low current density devices since the AlAs barrier thickness is 9 ML, compared to the 6 ML employed in previous devices. The devices, QWITT I and QWITT II, have drift region lengths of 1000Å and 2000Å, respectively.

2000Å	8.6 x 10^{18} cm^{-3}	InGaAs
100Å	1.3 x 10^{17} cm^{-3}	InGaAs
100Å	2.5 x 10^{16} cm^{-3}	InGaAs
15Å	Undoped	InGaAs
9 ML	Undoped	AlAs
47Å	Undoped	InGaAs
9 ML	Undoped	AlAs
15Å	Undoped	InGaAs
100Å	2.5 x 10^{16} cm^{-3}	InGaAs
100Å	1.3 x 10^{17} cm^{-3}	InGaAs
W	1.9 x 10^{17} cm^{-3}	InGaAs
2000Å	8.6 x 10^{18} cm^{-3}	InGaAs
	n+ InP substrate	

Fig. 4.10 Layer schematic of low σ AlAs/$In_{0.53}Ga_{0.47}As$ QWITTs with W = 1000Å (QWITT I) and W = 2000A (QWITT II).

The measured J - V characteristics of QWITT I and II are given in Fig. 4.11. The positive differential resistance (PDR) features apparent in the NDR region are due to the oscillating current. Although these features are present in previously discussed devices, they are not as dramatic as in Fig. 4.11.

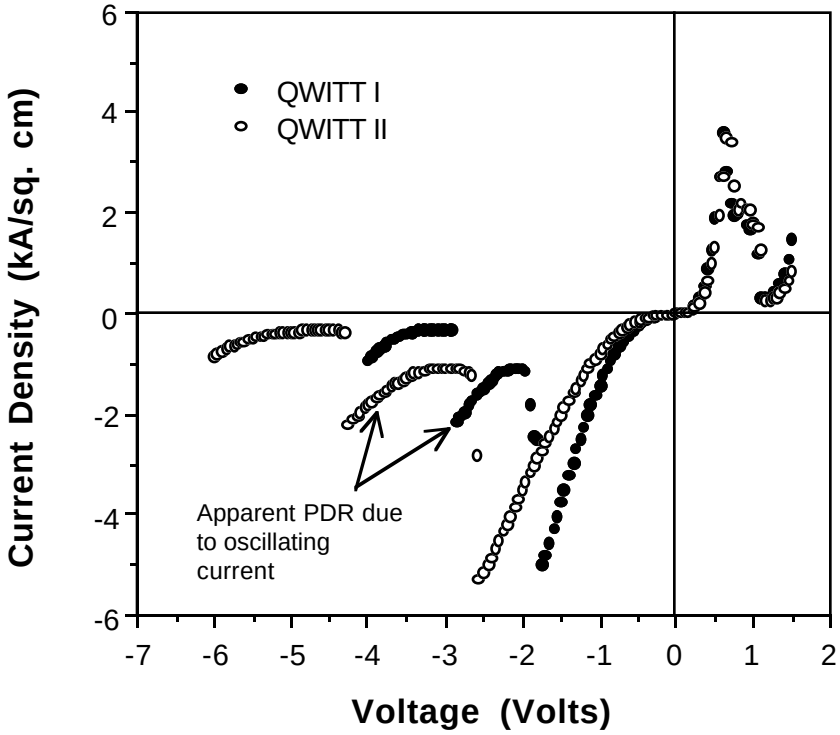

Fig. 4.11 Measured J - V characteristics of QWITT I (W = 1000Å) and QWITT II (W = 2000Å). The apparent positive differential resistance region between the peak and valley is due to the oscillating current.

The device parameters of interest J_p, PVCR, V_p, ΔV, and σ for QWITT I and II in reverse bias (QWITT mode) are given in Table 4.1.

Device Parameters	QWITT I	QWITT II
J_p (kA/cm^2)	5.1 +- 0.3	5.1 +- 0.6
PVCR	16.1 +- 0.5	15.8 +- 0.4
V_p (Volts)	-1.8 +- 0.04	-2.5 +- 0.03
ΔV (Volts)	-1.3 +- 0.04	-2.1 +- 0.08
σ (ohm-cm)$^{-1}$	-0.05	-0.04

Table 4.1 Device parameters for QWITT I (W = 1000Å) and II (W = 2000Å) biased in QWITT mode (reverse bias). Average values with one standard deviation are given.

Since the quantum well in both structures are nominally identical, J_p, PVCR, and σ are similar as expected. The extracted σ of - 0.05 (ohm-cm)$^{-1}$ is a factor of ten smaller than the high σ QWITTs discussed earlier and results in a W_{opt} of about 1.2 µm. Analysis of the J - V data with a Poisson solver showed that the actual depletion region lengths of QWITT I and II were 1200Å and 1800Å, respectively. Since these lengths are less than W_{opt}, the ratio of the ΔV's should be equal to the ratio of the depleted region lengths of the two devices. This ratio is approximately equal to 1.5 (1800Å/1200Å) which is in close agreement with the ratio of the measured ΔV's (2.1V/1.3V =1.6).

4.6 AlAs/$In_{0.53}Ga_{0.47}As$ Depletion Edge Modulated QWITT (DEMQWITT)

The W_{opt} for the low σ QWITTs discussed in the previous section is approximately 1.2 µm. Fabricating a QWITT structure with such a large W would be impractical for two reasons. First, given the magnitudes of the electric fields involved, it would be extremely difficult to completely deplete one micron. Second, the peak voltage would be extremely high and result in low DC-to-RF conversion efficiency oscillators. For oscillator applications, increasing the $\Delta V \Delta J$ product to improve the RF output power is the prime concern. However, it is also desirable to decrease V_p as this will reduce the required bias voltage and result in improved DC-to-RF conversion efficiency. This can be done by inserting a doping

spike (a heavily doped layer) between the quantum well and the drift region. A properly designed doping spike will reduce the electric field in the drift region but yet fully deplete the drift region. The end result is a reduction in V_p with ΔV remaining unchanged. Kesan *et al.* have employed this technique to reduce V_p and increase the conversion efficiency in AlAs/GaAs QWITTs [13].

Another approach can be taken to achieve the same goal of reducing V_p without sacrificing ΔV. Although this technique employs a doping spike, it is fundamentally different from the doping spike method. Recall that the quantum well injector characteristic can be extracted from the J - V curve by accounting for voltage drops due to series parasitic series resistance and space charge regions surrounding the double barrier structure. The injector characteristic for the AlAs/$In_{0.53}Ga_{0.47}As$ quantum well used in this study is shown in Fig. 4.12.

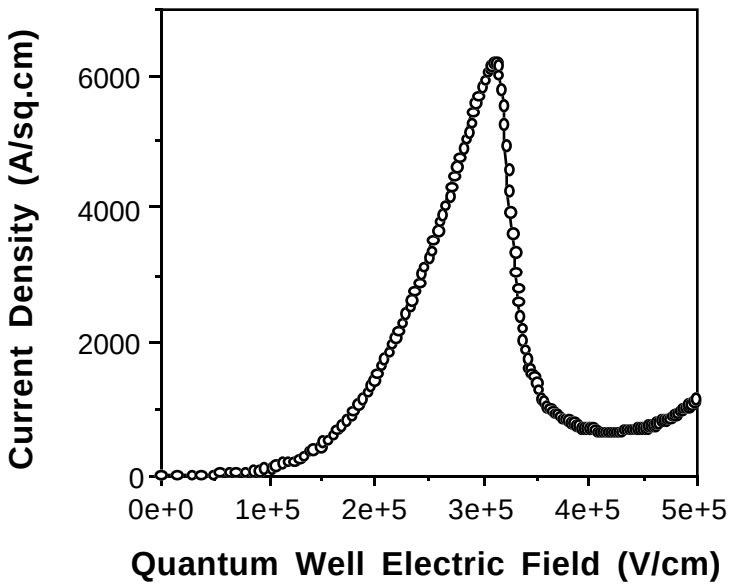

Fig. 4.12 Quantum well injector characteristic of AlAs/$In_{0.53}Ga_{0.47}As$ quantum well used in DEMQWITT study. Provided by K. Gullapalli.

From Eq. 4.12, W_{opt} is inversely proportional to the differential conductance of the injector characteristic. From Fig. 4.12 it is clear that near the peak, W_{opt} is small because of the high differential conductance. However, in much of the NDR region, the optimum length is very large because of the very low differential conductance. Therefore, by grading the doping profile in the drift region from high to low, it should be possible to obtain depletion region lengths that are optimum at each point in the NDR region of the injector characteristic. Note that such a design, where the depletion edge is modulated during the rf cycle, is very different from the conventional QWITT design where the depletion region length is fixed. Therefore, this device has been named the depletion edge modulated QWITT or DEMQWITT.

A DEMQWITT with the layer schematic shown in Fig. 4.13 was fabricated. The downstream layer doping profile consists of a 215Å, three step dopant transition layer adjacent to the AlAs barrier, a 210Å heavily doped spike layer, and finally a 1 μm thick, nominally undoped drift region. The background carrier concentration in the drift region is assumed to be n-type, 1×10^{16} cm^{-3}. The measured I - V characteristic in reverse bias (DEMQWITT mode) is shown in Fig. 4.14.

2000Å	7.1 x 10^{18} cm^{-3}	InGaAs
100Å	1.0 x 10^{17} cm^{-3}	InGaAs
100Å	2.1 x 10^{16} cm^{-3}	InGaAs
15Å	Undoped	InGaAs
9 ML	Undoped	AlAs
47Å	Undoped	InGaAs
9 ML	Undoped	AlAs
15Å	Undoped	InGaAs
100Å	2.1 x 10^{16} cm^{-3}	InGaAs
100Å	1.0 x 10^{17} cm^{-3}	InGaAs
L	1.0 x 10^{18} cm^{-3}	InGaAs
1 µm	1.0 x 10^{16} cm^{-3}	InGaAs
2000Å	7.1 x 10^{18} cm^{-3}	InGaAs
	n+ InP substrate	

Fig. 4.13 Layer schematic of AlAs/$In_{0.53}Ga_{0.47}As$ DEMQWITT. The doping spike thickness, L, is 210Å. The 1 µm layer is nominally undoped and assumed to be n-type, 1 x 10^{16} cm^{-3}.

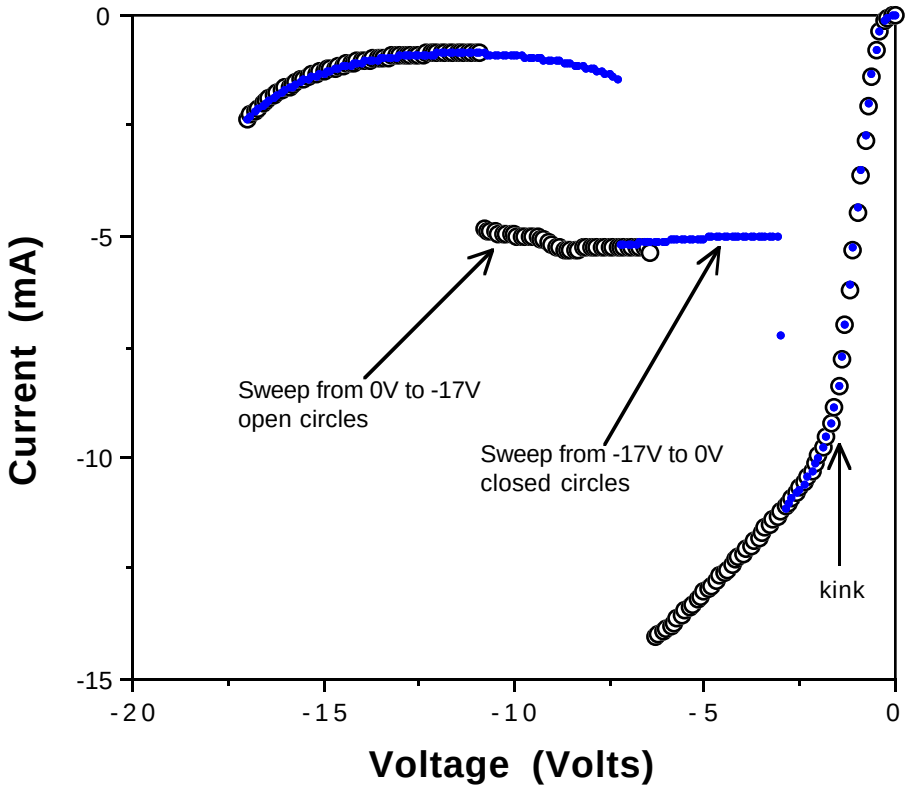

Fig. 4.14 Measured I - V characteristic of L = 210Å AlAs/$In_{0.53}Ga_{0.47}As$ DEMQWITT. The voltage is sweeped from 0V to -17V (open circles) and back to 0V (closed circles). The hysterisis is due to the difference in the start-up condition for oscillation and the space-charge resistance due to the 1 μm lightly doped drift region.

A few remarks should be made about the I - V curve. What is quite remarkable is the extended valley region, approximately ten volts. This is much larger than the two volts achieved with the low σ QWITTs discussed in the previous section. In the PDR region before the peak, the kink that appears as the PDR slope changes is due to the electric field being insufficiently screened by the doping spike layer. The region of the I - V curve between the kink point and the peak represents the electric field punchthrough into the lightly doped region.

Apparent in the figure is the hysterisis as the voltage is sweeped from 0V to -17 V and back to 0 V. This is due to the difference in the start-up condition for oscillation and the space-charge resistance due to the 1 μm lightly doped drift region. To improve the characteristics, the doping spike layer should either be thicker or have a higher doping concentration. Furthermore, the 1 μm drift region doping was probably lower than the assumed value of 1×10^{16} cm^{-3}.

Despite the spectacular ΔV available with the DEMQWITT, application to microwave oscillators is limited to low frequency (few GHz) operation by the device's low J_p. To avoid large peak voltages and possible catastrophic breakdown, DEMQWITTs can only be fabricated if the J_p is low enough that the electron concentration required to support J_p is less than the background doping concentration. Furthermore, the requirement that 1 μm be totally depleted places an upper limit on the background doping concentration, thus again limiting J_p. Nevertheless, the DEMQWITT is a promising device at low gigahertz frequencies for applications requiring high power, high efficiency operation.

4.7 Very High Efficiency Microwave Oscillators

The use of two terminal NDR devices as oscillators can be understood by considering the oscillator circuit shown in Fig. 4.15. R_D and X_D are functions of the bias voltage (not shown) and signal amplitude across the device and are assumed to be frequency independent. $Z(\omega)$ is the impedance looking into the resonant circuit and load. The condition for steady-state, free-running oscillation is given by the following celebrated equations known as the Kurokawa criterion [14]

$$R(\omega) + R_D = 0 \qquad (4.14)$$

$$X(\omega) + X_D = 0 \qquad (4.15)$$

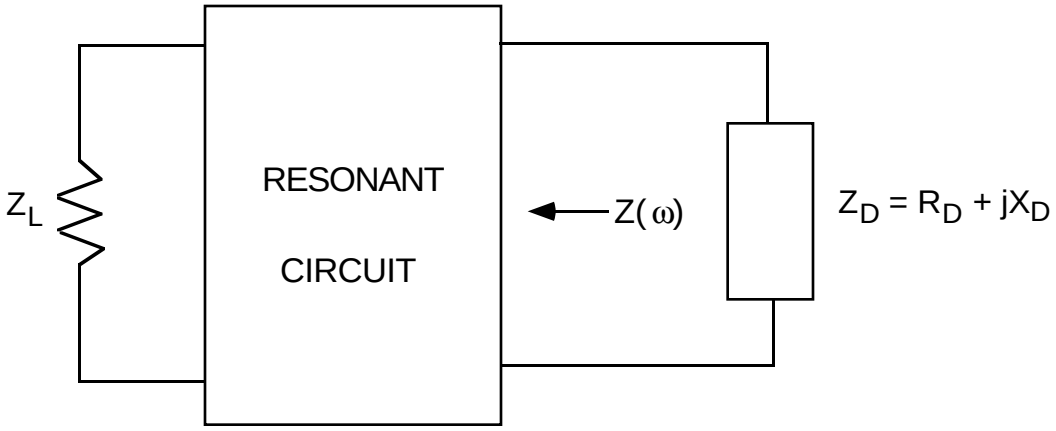

Fig. 4.15 Schematic diagram of oscillator circuit. $Z(\omega)$ is the impedance looking into the resonant circuit from the active device. Z_D and Z_L are the device and load impedance, respectively.

When the device is biased in the NDR region, R_D is negative and Eq. 4.14 can be satisfied. The frequency at which Eq. 4.15 is satisfied is the oscillation frequency while Eq. 4.14 determines the oscillation magnitude across the device and hence the power delivered to the load.

If the J - V characteristics of the low σ AlAs/$In_{0.53}Ga_{0.47}As$ QWITTs discussed in section 4.5 are examined carefully, one notices that the post-valley current does not rise as quickly as it does for the high σ AlAs/$In_{0.53}Ga_{0.47}As$ QWITTs. The typical voltage swing in NDR based oscillators extends past the NDR region into the PDR and the power output is proportional to the peak-to-peak voltage swing. Therefore, if the post valley current does not rise rapidly, the voltage swing will be larger and hence more power will be generated.

Based on this observation, these devices were placed in two open circuit single stub resonator circuits, which were designed using 50Ω microstrip lines for oscillation at 1 and 2.7 GHz. The microwave measurements were conducted by S. Javalagi and further details can be found in [15]. Both small signal and large signal calculations on the devices showed a very nearly real impedance for low

microwave frequencies (< 5 GHz). The open circuit stub in the circuit produces a real impedance at the device only over a narrow band of frequencies; thus the Kurokawa condition can be satisfied only in this frequency band. For the stub lengths chosen the circuit impedance should be purely real at about 1 and 2.7 GHz for circuits 1 and 2, respectively. Since the diode impedance is nearly real, the frequency of the oscillation is expected to be independent of the diode area or structure. The diodes were biased through a HP11612A bias tee and the DC port was monitored for bias line oscillations.

The diode mesas were contacted by a tungsten whisker at the end of the circuit and devices with different areas on each sample were probed. The RF output power was measured by placing each sample at the end of the circuit and varying the DC bias voltage until maximum output power was obtained. Particular care was taken to ensure the accuracy of the RF power and efficiency measurements by accounting for all parasitic losses in the measurement circuit and using a calibrated RF power meter. The experimental results for both QWITT 1 and QWITT 2 operating in the two circuits are summarized in Table 4.2.

Device	Circuit 1			Circuit 2		
	Freq. (GHz)	Power Density (kW/cm^2)	Efficiency η (%)	Freq. (GHz)	Power Density (kW/cm^2)	Efficiency η (%)
QWITT I	0.9	3.0	37	2.3	2.2	26
QWITT II	0.9	3.9	42	2.3	4.0	47

Table 4.2 Average values for power density and DC-to-RF power conversion efficiency using QWITT I and II in circuits 1 and 2. Results are averaged over four to five devices. Measurements done by S. Javalagi.

The large signal specific negative resistance of the device is a strong function of the RF amplitude, hence for a fixed RF circuit the power density varies with device area. The frequency spectrum of the QWITT oscillators was fairly narrow, producing a typical spectrum which was 15 dB down 5 kHz off the center

frequency for a resolution bandwidth of 1 kHz. The linewidth was limited by the very low Q circuit used here.

A DC-to-RF power conversion efficiency as high as 50 % was achieved with a power density of 4 kW/cm^2 on QWITT 1. To our knowledge, this is the highest efficiency ever reported for continuous wave operation with a two terminal device [16]. Conventional IMPATT diodes have been shown to have efficiencies of 60%, but only in a pulsed operation mode [17]. In CW operation IMPATTs have demonstrated efficiencies of 43% at the higher end and typically in the range of 16-36% [18]. Gunn diodes typically have DC to RF conversion efficiencies of less than 15% [19, 20]. The highest efficiency reported for quantum well diode oscillators, hitherto, has been 11% at a frequency of 1 GHz [21]. The maximum power obtained was 20 mW, which was achieved without any heat sinking. This is the highest power reported to date for quantum well diode oscillators. Such high power is possible since these QWITT diodes have very high specific negative resistance, allowing the use of very large area diodes without producing bias line oscillations.

4.8 Application of QWITTs to very high frequency oscillators

As discussed in the introduction, the development of high frequency DBRTD and QWITT oscillators has been driven by the need to develop solid-state sources at submillimeter wavelengths (frequencies greater than 300 GHz). The role of such a source would be to serve as the local oscillator (LO) in a heterodyne receiver system. In this frequency range, the LO power requirement of the mixer diode (typically a Schottky diode) in the receiver is about one milliwatt at 300K [22].

At such high frequencies, DBRTDs and IMPATTs are the only two devices that can even generate power. An output power of 200 μW at 361 GHz achieved with a silicon IMPATT has been reported by Ino *et al.* [23]. However, higher

frequency operation of IMPATTs is limited to approximately 500 GHz by the phase delay associated with the impact ionization process [24]. Therefore, the DBRTD remains as the only device with potential to generate the required output power.

In this chapter, we have discussed two techniques to increase the power output of DBRTDs. First, space-charge effects were profitably utilized in a modification of the DBRTD, the QWITT diode, to increase ΔV, the NDR voltage range. Second, by adopting the AlAs/$In_{0.53}Ga_{0.47}As$ material system, higher available current density (ΔJ) devices have been fabricated. To evaluate their high frequency performance requires, of course, that they be tested in actual oscillator circuits. However, performing oscillator experiments at frequencies at and above 100 GHz is extremely difficult and more of an art than science. In fact, as shown below, there are only a handful of research groups that have published DBRTD oscillator results at frequencies of 100 GHz and above. Therefore, we will review the state-of-the-art high frequency DBRTD oscillator results and compare the devices discussed in this work to those used in the oscillator experiments.

Shown in Fig. 4.16 are the state-of-the-art oscillator output powers versus oscillation frequency. Five sets of data are plotted for DBRTDs in the AlAs/$In_{0.53}Ga_{0.47}As$, AlSb/InAs, and AlAs/GaAs material systems. For frequencies below 100 GHz, the output powers reported are below 100 mW with the highest output power of 20 mW at 1 GHz reported by our group (discussed in the previous section). In this frequency range, DBRTDs are not competitive since IMPATTs, GUNN diodes, and field-effect transistors can produce much higher output powers [25].

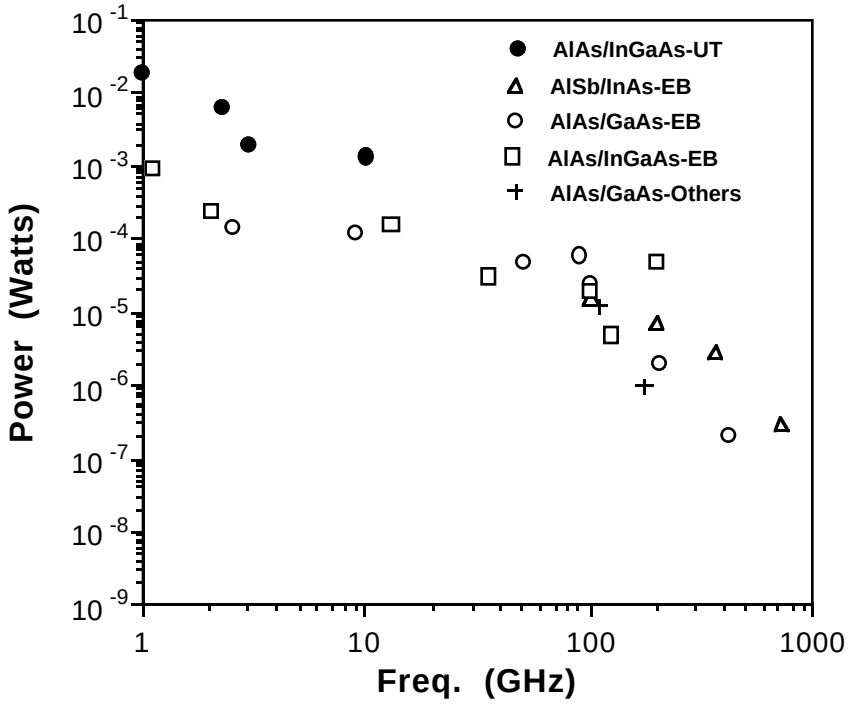

Fig. 4.16 State-of-the-art results for DBRTD oscillator output power versus frequency. Five sets of data are plotted for DBRTDs in the AlAs/$In_{0.53}Ga_{0.47}As$, AlSb/InAs, and AlAs/GaAs material systems. The AlAs/$In_{0.53}Ga_{0.47}As$-UT results (solid circles) are from the low σ devices discussed in section 4.5 and will be covered in further detail in the next section. The AlAs/$In_{0.53}Ga_{0.47}As$-EB data (open triangles) [26, 27], the AlAs/GaAs-EB data (open circles) [28], and the AlSb/InAs results (open squares)[29] were reported by Brown *et al.* . The data represented by crosses (AlAs/GaAs-Others) is from [30] and [31].

At frequencies above 100 GHz, the output power falls rapidly to hundreds of nano-watts. The highest frequency achieved is 712 GHz by Brown *et al.*, with an output power of 300 nW [21]. Although this is an impressive result, it is still not sufficient to satisfy the LO power requirement of the Schottky diode mixer discussed earlier. Further, the claim of fundamental oscillation at 712 GHz by Brown *et al.* is controversial and the evidence of fundamental oscillation is tenuous

at best. The 712 GHz frequency may actually be the second harmonic of a 356 GHz fundamental oscillation.

The question to be asked is whether or not further improvements in DBRTD and QWITT performance are possible. The frequency response, as discussed in section 4.2, depends on the magnitude of the characteristic frequency, σ/ε. It is desirable to operate in the " low frequency" regime where ω (frequency of operation) $<< \sigma/\varepsilon$ and avoid the rapid ω^{-3} fall-off when $\omega >> \sigma/\varepsilon$. Therefore, σ/ε should be at least as large as the desired oscillation frequency to maintain reasonable output powers. The extracted σ from the AlAs/$In_{0.53}Ga_{0.47}As$ and AlSb/InAs devices of Brown *et al.* shown in Fig. 4.16 along with the extracted σ's from devices presented in this work are tabulated below

Device Description	σ (ohm-cm)$^{-1}$	$f = \sigma/2\pi\varepsilon$ (GHz)	Oscillator Results	Ref.
AlSb/InAs with 5 ML barriers and 64Å quantum well.	-1.7	215	300 nW @712 GHz	[28]
AlAs/$In_{0.53}Ga_{0.47}As$ with 5 ML barriers and 61Å quantum well.	-1	140	50 µW @200GHz.	[26]
AlAs/$In_{0.53}Ga_{0.47}As$ with 5 ML barriers and 50Å quantum well.	-1.3	180	Not measured	This work.

Table 4.3 Comparison of extracted σ, characteristic frequency, σ/ε, and high frequency oscillator results of high current density devices fabricated in the AlAs/$In_{0.53}Ga_{0.47}As$ and AlSb/InAs material systems.

The oscillator results presented in Table 4.3 are state-of-the-art and it is not obvious if they can be improved upon. To get an idea of the difficulty of obtaining power at submillimeter wavelengths, we can do a simple calculation taking into account circuit impedance matching requirements. Assume that the oscillation

frequency is 800 GHz. Further, assume that the optimum quantum well injection conductance for the frequency of operation is available and is given by [4]

$$\left|\sigma_{opt}\right| = \frac{\omega\varepsilon}{\sqrt{3}} \tag{4.16}$$

Plugging this value of σ (equal to 3.5 (ohm-cm)$^{-1}$ at 800 GHz) into Eq. 4.4 for the drift region negative resistance and into the expression for the quantum well specific negative resistance [4]

$$R_{QW} = \frac{L_{QW}}{\sigma}\left[1 + \left(\frac{\omega}{\sigma/\varepsilon}\right)^2\right]^{-1} \tag{4.17}$$

One finds that the specific negative resistance available is equal to 4 x 10^{-8} (ohm-cm^2), where L_{QW} = 80Å, v_{sat} = 10^7 cm/s, and ε = 1.2 x 10^{-12} F/cm. The negative resistance available at the terminals of the device is equal to the negative resistance from Eqs. 4.4 and 4.17, R_{device}, plus the positive resistance due to ohmic contacts, undepleted spacer regions, and the heavily doped contact regions. All these positive resistance terms can be lumped into a specific positive resistance, R_{par}, as they scale with area. If the resistance of the external circuit is r_{circ}, then impedance matching requirements require that the magnitude of the negative resistance at the device terminals equal r_{circ}

$$r_{circ} = \frac{\left(R_{device} + R_{par}\right)}{A} \tag{4.18}$$

where A is the device area. Assuming that a 1 ohm circuit impedance can be achieved along with R_{par} = 10^{-7} (ohm-cm^2), we find, from Eq. 4.18, that the device area required for circuit impedance matching is equal to 4 x 10^{-8} cm^2. If we assume that the oscillator output power is equal to

$$P_{out} = \frac{A}{4}\Delta V \Delta J \qquad (4.19)$$

where $\Delta V = 0.25$ V, $\Delta J = 350$ kA/cm^2, and $A = 4 \times 10^{-8}$ cm^2, then $P_{out} = 875$ μW. This output power is still lower than the 1 mW LO requirement of the Schottky diode mixer.

The R_{par} and r_{circ} values used in the above calculation are extremely optimistic and extremely difficult to achieve at 800 GHz. Furthermore, coupling losses from the device terminals to the input of the mixer have not been considered and can reduce the power by at least a factor of two. Given these considerations along with the state-of-the-art DBRTD oscillator results reported in Table 4.3, it appears that generation of useful amounts of power by DBRTD fundamental oscillators is not viable and alternative techniques must be pursued. One such technique which will be discussed in the next chapter is frequency multiplication with a varactor diode.

4.9 Summary

We have described the operation of the Quantum Well Injection Transit (QWITT) diode. This device offers a larger ΔV and hence larger negative resistance than a baseline DBRTD, both of which can lead to higher output powers. In fact, the benefits of optimizing for ΔV are twofold. First, for a given ΔJ, the power density product $\Delta V \Delta J$ is maximized. Second, the specific negative resistance is maximized, which maximizes the device area that can be used for a given circuit impedance. Therefore, for a given quantum well design, by adopting the QWITT design principles, maximum power can be obtained without sacrificing the frequency response. The enhanced ΔV is achieved by modifying the downstream spacer layer profile to take advantage of space-charge effects arising from carriers traversing a space-charge region at a constant saturation velocity. High current density AlAs/$In_{0.53}Ga_{0.47}As$ QWITTs were fabricated and characterized. The corresponding optimum drift region length, W_{opt}, and the

extracted quantum well injection conductance, σ, were found to be about 900Å and -0.57 $(ohm\text{-}cm)^{-1}$, respectively, for 6 ML thick AlAs barriers. Catastrophic breakdown was found to occur in the high current density AlAs/$In_{0.53}Ga_{0.47}As$ QWITTs if the drift region doping was lower than the drift region electron concentration.

Low sigma AlAs/$In_{0.53}Ga_{0.47}As$ QWITTs were also characterized. These devices exhibit ΔV's of two volts and exhibit a very slowly rising post-valley current. This feature is necessary for generating large voltage amplitudes during oscillation. Microwave oscillators utilizing these diodes were tested and a CW DC-to-RF power conversion efficiency of 50% was achieved. This is the highest efficiency reported for CW operation of a two terminal semiconductor device. Also, output powers as high as 20 mW was obtained, a record for DBRTD oscillators. The W_{opt} for these low sigma structures is approximately 1.2 μm, a distance too large to deplete with conventional quantum well and spacer layer design. In an effort to fabricate devices with very large ΔV, a novel low-hi-low drift region doping profile was adopted which provides a W_{opt} at each point in the NDR region of the quantum well injector characteristic. Such a device where the depletion edge is modulated during the rf cycle, is named the depletion edge modulated QWITT or DEMQWITT. An AlAs/$In_{0.53}Ga_{0.47}As$ DEMQWITT was fabricated and a valley region as large as ten volts was achieved.

For very high frequency operation, high σ's are required which result in very low specific negative resistance. Although, the QWITT approach will maximize the negative resistance, given the constraints of external circuit matching and power coupling, generation of useful amounts of power by fundamental oscillation with DBRTDs is not presently viable and alternative techniques must be pursued. One promising technique, to be discussed in the next chapter, is frequency multiplication with a varactor diode.

References

[1] V. P. Kesan, D. P. Neikirk, B. G. Streetman, and P. A. Blakey, " A new transit-time device using quantum well injection," IEEE Electron Device Lett., vol. 8, No. 4, pp.129-131, 1987.

[2] K. Gullapalli, V. K. Reddy, D. R. Miller and D. P. Neikirk, " Analysis of Space Charge Effects in Resonant Tunneling Diodes," unpublished.

[3] K. K. Gullapalli, A. J. Tsao, and D. P. Neikirk, " Observation of zero-bias, multi-state behavior in selectively doped two-terminal quantum tunneling devices," 1992 IEDM Digest, pp.479-482, 1993.

[4] Vijay P. Kesan, Dean P. Neikirk, Peter A. Blakey, Ben G. Streetman, and Thomas D. Linton, " The Influence of Transit-Time Effects on the Optimum Design and Maximum Oscillation Frequency of Quantum Well Oscillators," IEEE Trans. on Electron Devices, vol. 35, No. 4, pp.405-413, 1988.

[5] Chai Yeh, " A Unified Treatment of the Impedance of Transit-Time Devices," IEEE Trans. on Education, vol. 28, No. 3, pp.117-124, 1985.

[6] S. M. Sze, " Physics of Semiconductor Devices, 2nd ed.," Wiley-Interscience, 1981.

[7] K. K. Gullapalli, " Simulation of Electron transport in Double Barrier Diodes, Master's Thesis," Aug. 1991.

[8] Sadao Adachi, " GaAs, AlAs, AlxGa1-xAs: Material parameters for use in research anddevice applications," J. Appl. Phys., vol. 58, No. 3, pp.R1-R29, 1985.

[9] T. H. Windhorn, L. W. Cook, and G. E. Stillman, " The Electron Velocity-Field Characteristic for n-$In_{0.53}Ga_{0.47}As$ at 300K," IEEE Electron Device Lett., vol. 3, No. 1, 1982.

[10] I. Mehdi, R. K. Mains, and G. I. Haddad, " Effect of spacer layer thickness on the static characteristics of resonant tunneling diodes," Appl. Phys. Lett., vol. 57, No. 9, pp.899-901, 1990.

[11] Private communication with Kiran Gullapalli, November 1993.

[12] C. R. H. White, M. S. Scolnick, L. Eaves, and M. L. Leadbeater, " Electroluminescence and impact ionization phenomena in a double-barrier resonant tunneling structure," Appl. Phys. Lett., vol. 58, No. 11, pp.1164-1167, 1991.

[13] V. P. Kesan, A. Mortazawi, D. R. Miller, V. K. Reddy, D. P. Neikirk, and T. Itoh, " Microwave and Millimeter-Wave QWITT Diode Oscillators," IEEE Trans. on Micro. Theory and Tech., vol. 37, No. 12, pp.1933-1941, 1989.

[14] K. Kurokawa, " Some Basic Characteristics of Broadband Negative Resistance Oscillator Circuits," The Bell System Tech. Journal, pp.1937-1955, 1969.

[15] S. Javalagi, " High power and high efficiency quantum well oscillators," M. S. Thesis, The University of Texas at Austin, December 1991.

[16] S. Javalagi, V. Reddy, K. Gullapalli, and D. Neikirk, " High Efficiency Microwave Diode Oscillators," Electronics Lett., vol. 28, No. 18, pp.1699-1701, 1992.

[17] K. N. Chang, " Avalanched diodes as UHF and L-band sources," RCA Review., 1969, vol. 30, pp. 3 - 14.

[18] J. W. Gewartowski, "Progress with CW IMPATT Diode circuits at Microwave Frequencies," IEEE Trans. on Microwave Theory and Tech., Vol. 27, No. 5, May 1979, pp. 434-442

[19] F. B. Frank and G.F. Day, "High CW power K-band Gunn oscillators," Proc. IEEE, Vol. 57, 1969, p.339

[20] K. Chang, Ed., Handbook of Microwave and Optical Components: Vol. 2. New York: Wiley, 1990, pp. 298-299

[21] E. R. Brown, C. D. Parker, A. R. Calawa, M. J. Manfra, T. C. L. G. Sollner, C. L. Chen, S. W. Pang, and K. M. Molvar, " High-speed resonant tunneling diodes made from the InGaAs/AlAs material system," SPIE vol. 1288 on High Speed Electronics and Device Scaling, 1990, pp. 122-135

[22] Antii V. Raisanen, " Frequency Multipliers for Millimeter and Submillimeter Wavelengths," Proc. of the IEEE, vol. 80, No. 11, pp.1842-1852, 1992.

[23] M. Ino, T. Ishibashi, and M. Ohmori, " C.W. oscillation with p+ - p - n+ silicon IMPATT diodes in 200 GHz and 300 GHz bands," Electronics Lett., vol. 12, No. 6, pp.148-149, 1976.

[24] P. A. Blakey and R, K, Froelich, " Fundamental high-frequency performance limit for IMPATT mode operation," Electronics Lett., vol. 21, No. 1, pp.28-29, 1985.

[25] Y. C. Shih and H. J. Kuno, " Solid-State Sources from 1 to 100 GHz," Microwave Journal: State-of-the-Art Reference, pp.145-161, 1989.

[26] E. R.Brown, C. D. Parker, K. M. Molvar, and K. D. Stephan, " A quasioptically stabilized resonant-tunneling diode oscillator for the millimeter-and submillimeter-wave regions," IEEE Trans. on Microwave Theory and Tech., vol. 40, No. 5, pp. 846-850, 1992.

[27] E. R. Brown, C. D. Parker, A. R. Calawa, M. J. Manfra, and K. M. Molvar, " A quasi-optical resonant-tunneling diode oscillator operating above 200 GHz," IEEE Trans. on Microwave Theory and Tech., vol. 41, No. 4, pp.720-722, 1993.

[28] E. R. Brown, T. C. L. G. Sollner, C. D. Parker, W. D. Goodhue, and C. L. Chen, " Oscillations up to 420 GHz in GaAs/AlAs resonant tunneling diodes," Appl Phys. Lett., vol. 55, No. 17, pp.1777-1779, 1989.

[29] E. R. Brown, J. R. Soderstrom, C. D. Parker, L. J. Mahoney, K. M. Molvar, and T. C. McGill, " Oscillations up to 712 GHz in InAs/AlSb resonant-tunneling diodes," Appl. Phys. Lett., vol. 58, No. 20, pp.2291-2293, 1991.

[30] H. Gronqvist, A. Rydberg, H. Hjelmgren, H. Zirath, E. Kollberg, J. Soderstrom, and T. Andersson, " A millimeter wave quantum well diode oscillator," Proc. of 18th European Microwave Conference, 1988.

[31] O. Vanbesien, R. Bouregba, P. Mounaix, D. Lippens, L. Palmateer, J. C. Pernot, G. Beaudin, P. Encrenax, E. Bockenhoff, J. Nagle, P. Bois, F. Chevoir, and B. Vinter, " Resonant tunneling diodes as sources for millimeter and submillimeter wavelengths," Proc. of Third International Symposium on Space Terahertz Technology," pp.548-560, March 24-26, 1992.